Journal of Sound and Vibration (1999) **228**(5), 1057–1078
Article No. jsvi.1999.2458, available online at http://www.idealibrary.com on IDEAL®

EFFICIENT VIBRATION MODELLING OF ELASTIC VEHICLE TRACK SYSTEMS

C. SCHOLAR AND N. C. PERKINS

Department of Mechanical Engineering and Applied Mechanics, The University of Michigan, Ann Arbor, MI 48109-2125, *U.S.A.*

(*Received* 30 *September* 1998, *and in final form* 11 *June* 1999)

A vehicle track model is developed with the objective of providing new capabilities in modelling track vibration response. Understanding track vibration is essential to evaluating the durability of track components and the vibration energy transmitted to the vehicle. A new element model is derived herein that represents a track span as a continuous elastic member with distributed inertia. This model captures the effects of static track sag, static track tension, and the coupling of longitudinal and transverse track vibration. Results from a companion experimental study on a section of track are reviewed and support the use of this continuum approximation over a well-defined frequency spectrum. The track element model is then extended to describe an entire track circuit for an example military vehicle. An eigenanalysis of this circuit model leads to the system vibration modes that are subsequently employed in a low order model for forced response. The forced response characteristics resulting from two major excitation sources, roadarm motion and polygonal action, are described. The modal content of the track response is then examined to determine the minimum size model required to describe low-frequency track vibration. It is concluded that such low order system models offer an efficient alternative to established large degree-of-freedom multi-body track models.

1. INTRODUCTION

Models of mechanical systems involving closed kinematic chains, such as vehicle track models, utilize a variety of representations for the chain itself. As one example, tank track applications involve on the order of 80 chain links (pitches) which form a continuous track that engages with the drive sprocket, idler wheel, road wheels and support rollers; refer to Figure 1. The road wheels are mounted on torsion-bar roadarms providing suspension to the vehicle.

This suspension provides some isolation from terrain-induced vibration. Nevertheless, very significant vibration levels remain, both in the track where they influence the durability of track components, and in the hull where they degrade the performance of on-board instrumentation, electronics, and personnel. The track is a major source of this vibration energy.

There are two dominant modes of track vibration: transverse and longitudinal. Transverse track vibrations generate deformation normal to the track span and in

0022-460X/99/501057 + 22 $30.00/0

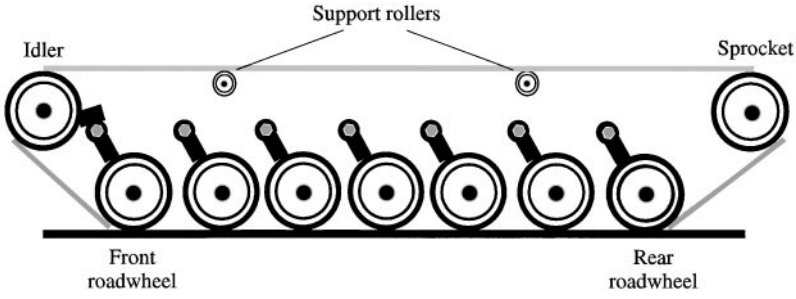

Figure 1. Track circuit schematic.

the vertical plane. This deformation requires relative rotation of adjacent pitches through rotation about the connecting pin/bushing assembly. Transverse track vibrations are readily visible and may also reach amplitudes sufficiently large to produce impacts of the track with the underside of the hull (sponson). Longitudinal track vibrations generate deformation tangent to the track span and require the relative separation of adjacent pitches through the radial compliance of the pin/bushing assembly. Longitudinal vibrations produce dynamic track tension and may promote bushing failure. These two modes of vibration are coupled, in general, due to the small static sag of the tensioned track. Note that the term "track vibration" used in this paper refers to the vibration of the track strand and not specific components *within* the track strand, such as the centerguide, bushings, pins, shoes, etc.

There are multiple sources of excitation to the track. At the track–terrain interface, the front and rear roadwheels provide motion at the boundary of the upper track spans. Rigid-body vehicle motion generates inertial loading for the entire circuit. Both of these sources can produce substantial vibration at lower frequencies. In a higher frequency spectrum proportional to vehicle speed, the track is excited by the drive sprocket, idler and other elements through polygonal action (pitches conforming to a polygon) as well as impact.

Early investigations of tracked vehicle modelling focused on kinematic track effects assuming negligible track inertia. These early models, therefore, cannot capture track vibration. Wheeler [1] incorporates a quasi-static model for track stretching to approximate the vertical forces of wheel–ground interaction. Garnich and Grimm [2] use the same track model but account for the effects of track bridging, drive sprocket interaction, and a track compensating linkage. Bennett and Penny [3] extend the quasi-static model by accounting for initial slack (sag) of the track. McCullough and Haug [4] developed a tracked vehicle model assuming quasi-static track response, referred to as the track super-element, in which rigid-body equations of motion are efficiently derived for systems containing recurring subsystems. Track tensions are derived from catenary cable equations and bridging effects. Dhir and Sankar, in developing a high-speed tracked vehicle model [5], also approximate track loads by considering the quasi-static stretching of a massless belt.

Tracked vehicle models also exist in which each pitch, sprocket, wheel and roller is assigned the requisite degrees of freedom (d.o.f.) in forming a large multi-body dynamic system. Choi [6] presents such a multi-body dynamic model in which the track consists of individual links connected by single d.o.f. revolute joints.

Highly detailed models of this nature have also been developed for the U.S. Army Tank Automotive Command by Wilcox [7, 8] and analyze track motion and track–sprocket interaction to high fidelity. Similarly, models by Galaitsis [9] employ a multi-body representation for the tracked vehicle model which is subsequently used to predict dynamic track loads during flat terrain traversal. These multi-body representations, while complete, frequently yield models containing several hundred d.o.f., which is presently impractical for use in real-time simulation.

The purpose of this paper is to present an alternative track model which can be used to support rapid simulations of tracked vehicle dynamics at frequencies characteristic of track vibration. The model developed herein considers the track as a continuum and captures both transverse and longitudinal track vibration. Solution efficiency derives from the use of classical modal co-ordinates. A linear model containing both continuous and discrete elements is derived that governs the coupled response of the track and the rotational response of the drive sprocket, road and idler wheels and support rollers. Roadarm motions and polygonal action are included as example excitation sources.

The outline of this paper is as follows. First, a description of the continuum element used to model the dynamics of the free track spans is presented. Second, results from an experiment on a section of track are reviewed and support the use of the continuum element over a well-defined frequency spectrum. Next, a track circuit model combining discrete and continuum elements is assembled in the context of an example application. An eigenanalysis of this circuit model leads to the modes that are subsequently used to evaluate forced response characteristics. Example results are provided which show that low-order tracked vehicle models can be used to capture low-frequency track vibration response.

2. ELEMENT MODEL

A continuum model is employed which describes the in-plane dynamics of a massive but flexible track sagging under its own weight.

With reference to Figure 2, this continuum model represents one span of the track circuit shown in Figure 1 and reduces to that of a shallow sag cable [10]. The co-ordinates $U(S, T)$ and $V(S, T)$ denote, respectively, longitudinal and transverse span displacements about an equilibrium configuration. S is an independent span co-ordinate defined on the domain $S \in [0, L]$, where L is span length. T denotes time. The equilibrium configuration can be assumed to be a parabola since the track satisfies the small sag condition $KL < 1$ where K is the curvature of the equilibrium configuration; refer to Irvine and Caughey [10] and Perkins [11].

The equations of motion for free in-plane motion about this equilibrium are derived in reference [11] which, after linearization, become

$$v_t^2 L\left[U_{,S} - \frac{k}{L}V\right]_{,S} = \frac{1}{g}U_{,TT}, \tag{1}$$

$$v_t^2 L V_{,SS} + k v_t^2\left[U_{,S} - \frac{k}{L}V\right] = \frac{1}{g}V_{,TT}, \tag{2}$$

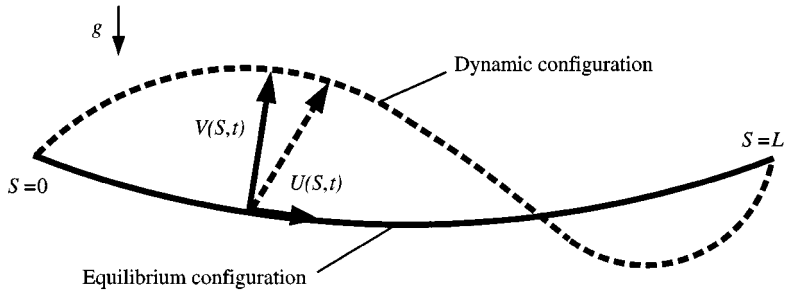

Figure 2. Element schematic.

with the non-dimensional parameters

$$v_l^2 = \frac{EA}{\rho g L}, \qquad v_t^2 = \frac{P_o}{\rho g L}, \qquad k = KL. \tag{3}$$

Here, EA is the track section modulus, ρg denotes the track weight/length, and P_o is the static track tension. The quantities v_l, v_t, and k have the interpretation of the (non-dimensional) speed of propagation of longitudinal waves, speed of propagation of transverse waves and equilibrium curvature, respectively.

In a typical track application, the speed of propagating waves in the longitudinal and transverse directions are quite disparate, with that in the longitudinal direction being much larger than that in the transverse direction; $v_l \gg v_t$. In the light of this fact, the model below further assumes that longitudinal waves in the track propagate sufficiently faster than transverse waves that the track *stretching* can be considered quasi-static. Thus, equation (1) governing longitudinal motion of the track can be approximated by one of statics, namely,

$$\left[U_{,S} - \frac{k}{L} V \right]_{,S} \cong 0. \tag{4}$$

Equation (4) can be integrated twice to yield an explicit expression for the longitudinal component $U(S, T)$,

$$U_{,S} - \frac{k}{L} V = F(T), \tag{5}$$

$$U(S, T) = F(T)S + \frac{k}{L} \int_0^S V(\eta, T)\, \mathrm{d}\eta + G(T), \tag{6}$$

where $F(T)$ and $G(T)$ are functions of integration. The coupling between the longitudinal and transverse motions is preserved through the integral term in equation (6). Equation (5) can be substituted into equation (2) to eliminate U from the transverse equation of motion leaving

$$v_t^2 L V_{,SS} + k v_l^2 F(T) = \frac{1}{g} V_{,TT}. \tag{7}$$

Consider next separate solutions of the form

$$U(S, T) = \bar{U}(S)e^{i\omega T}, \quad V(S, T) = \bar{V}(S)e^{i\omega T}, \quad F(T) = \bar{F}e^{i\omega T}, \quad G(T) = \bar{G}e^{i\omega T}, \tag{8}$$

with ω being a natural frequency. Substitution of equation (8) into equation (6) and (7) yields

$$\bar{U}(S) = \bar{F}S + \frac{k}{L}\int_0^S \bar{V}(\eta)\,d\eta + \bar{G}, \tag{9}$$

$$v_t^2 L\bar{V}'' + kv_l^2\bar{F} + \frac{\omega^2}{g}\bar{V} = 0. \tag{10}$$

The general solution to this "time-reduced" transverse equation of motion (10) is

$$\bar{V}(S) = A\sin(aS) + B\cos(aS) - \frac{gkv_l^2\bar{F}}{\omega^2}, \quad a = \frac{\omega}{v_t\sqrt{gL}}, \tag{11, 12}$$

where A and B are constants. Appropriate boundary conditions applied to equations (9) and (11) will complete the single span model which is then extended to the multi-span track circuit model of section 4.1. Free and forced vibration analyses of the complete circuit are described in sections 4.2 and 4.3.

3. EXPERIMENTAL VALIDATION

3.1. EXPERIMENTAL APPARATUS AND PROCEDURE

The modelling of a track (composed of a finite number of pitches) by an equivalent continuum is novel and requires justification. To this end, a series of experiments were performed on a representative (7-pitch) track span. The purpose of these tests was to determine how well the continuum element model describes the low-frequency physics of the track.

The test span shown in Figure 3 is rigidly supported at the left end and connected to a load cell and a hydraulic actuator at the right end; refer to Figure 4(a). The span is instrumented between the 2nd and 3rd pitches from the left with two track-mounted accelerometers, one aligned in the longitudinal direction, the other in the transverse direction; refer to Figure 4(b).

The track is tensioned to a desired static level, varying between 10 000 (44 545 N) and 20 000 lbs (89 091 N), prior to the addition of any excitation. The test span is then excited with a controlled harmonic longitudinal displacement input provided by the actuator. The input force is measured from the load cell and combined with the accelerometer signals to compute the track frequency response over a frequency range of 0–140 Hz using standard techniques. Through means of the small sag in the track span developed under its own weight, vibrations in the transverse and longitudinal directions are coupled. Thus, track resonances consisting largely of transverse motion can be easily excited via longitudinal input. Using the small sag

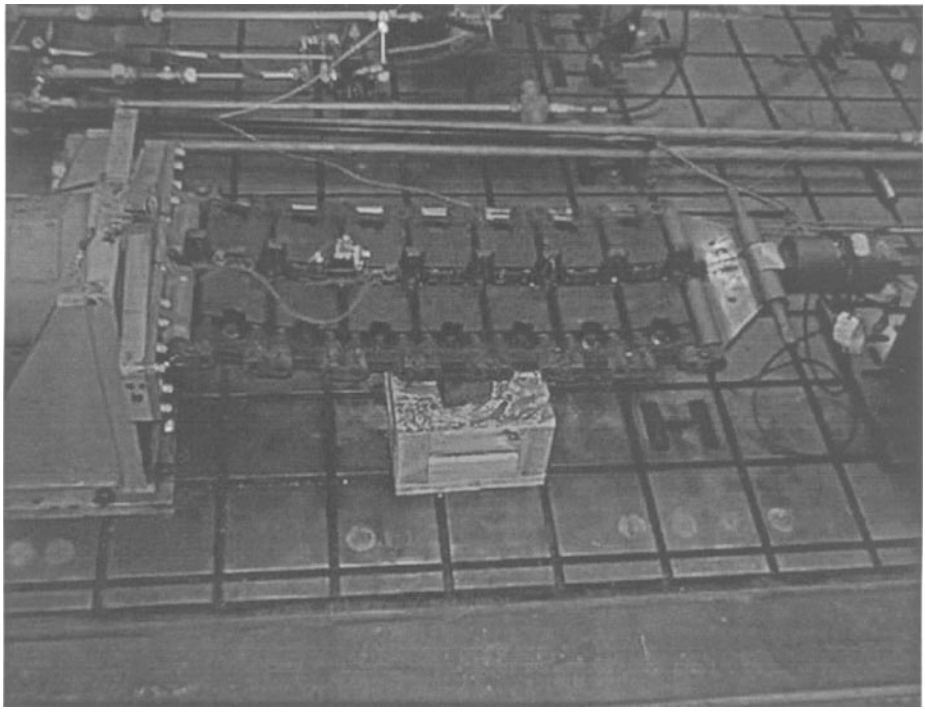

Figure 3. Experimental test stand; 7-pitch track for example vehicle.

cable theory as an approximation to the track span, the resonant frequencies of the simply supported track span can be readily predicted; see, for example, Irvine and Caughey [10]. To this end, the characteristic equation follows from equations (9) and (11) upon using the boundary conditions, $\bar{U}(0, T) = \bar{U}(L, T) = \bar{V}(0, T) = \bar{V}(L, T) = 0$.

3.2. EXPERIMENTAL RESULTS

Figure 5(a) shows the measured track frequency response obtained using the vertical accelerometer for the case of 15 000 lbs (66 818 N) static tension. Discernible peaks mark the natural frequencies of the first four span modes. Table 1 compares these measured frequencies to those predicted with the cable theory. The theory provides excellent agreement for the first two frequencies, an 8% error for the third, and a 18% error for the fourth. The errors for the third and fourth modes derive from omitting track bending rigidity (torsional stiffness of bushings used in pin connectors) which plays an increasingly important role in stiffening the track for higher order modes. However, as will be shown in section 4.2, many low order system modes of the full track circuit are well described using just the first two (component) modes of each track span. Moreover, the experimental results suggest that the continuum model is accurate to within 10% (for computed strand frequencies) when $\lambda \geqslant 2{\cdot}5L_{pitch}$, where λ is the distance between nodes for a vibration mode and L_{pitch} is the length of one track pitch.

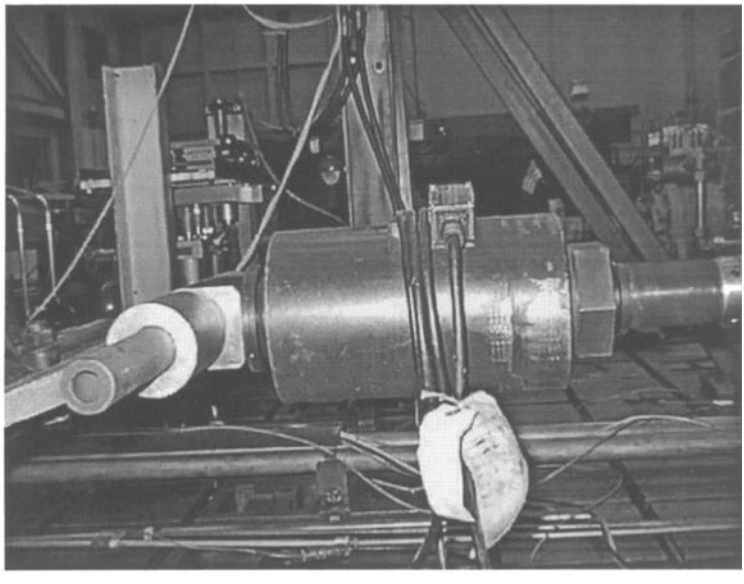

(a)

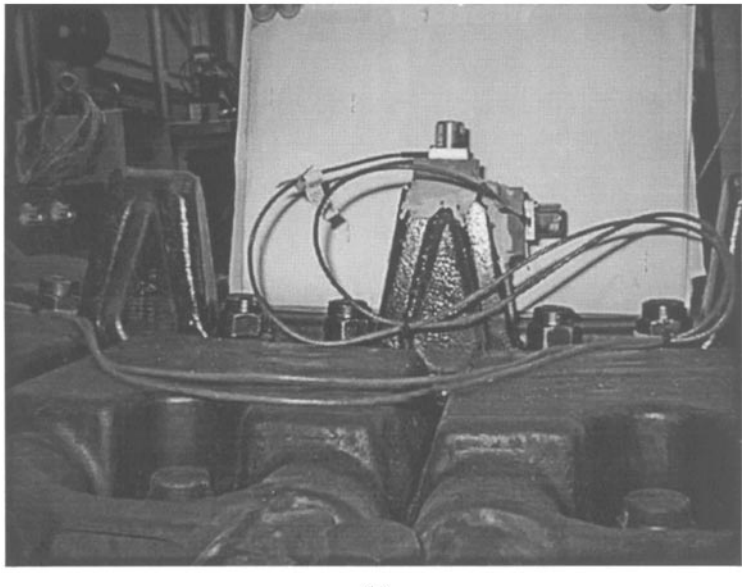

(b)

Figure 4. Experimental hardware: (a) load cell and connection to track span actuator; (b) track mounted accelerometers.

Figure 5(b) is the corresponding frequency response obtained using the horizontal accelerometer for the same test. The low-frequency resonances associated with large transverse track response can again be identified along with the clear broad resonance centered around approximately 110 Hz. This is the

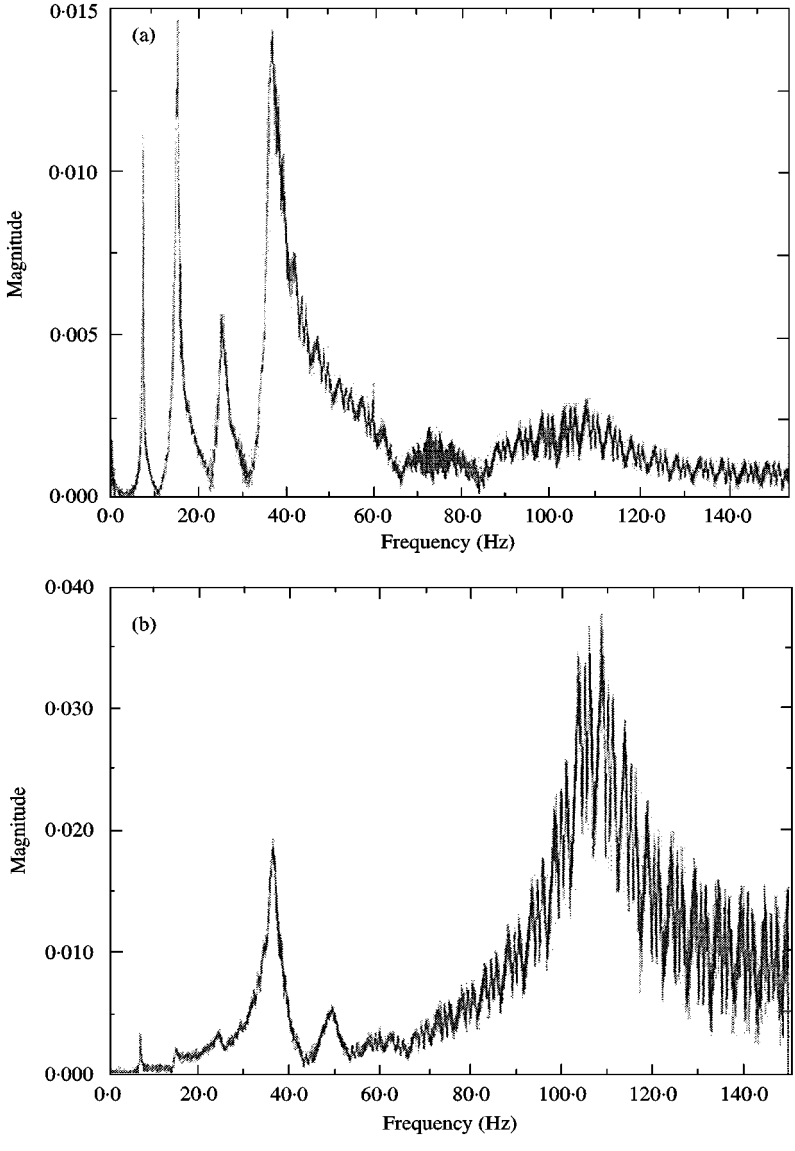

Figure 5. Experimental frequency responses: (a) vertical accelerometer; (b) horizontal accelerometer; 15,000 lbs tension.

natural frequency for the fundamental longitudinal mode for the test span and can be predicted very well by an equivalent classical (fixed–fixed) rod model; see, for example, Scholar and Perkins [12]. Because the sagged cable theory employed in this model treats track stretching as quasi-static, this type of resonance is not presently captured. Thus, the model developed will be used to analyze dynamics in the low- to mid-frequency range below the natural frequency of the first longitudinal mode.

TABLE 1

Comparison of natural frequencies

	Experiment (Hz)	Theory (Hz)
f_1	7·2	7·2
f_2	14·7	14·6
f_3	25·3	23·2
f_4	37·0	29·7

4. TRACK CIRCUIT MODEL

4.1. FORMULATION

The element model describing the dynamics in a single track span is now extended to form a model for the entire track circuit. This is done herein in the context of an example application of a vehicle possessing 5 upper spans, as illustrated in the schematic of Figure 6.

Notation for the circuit model is shown in Table 2. Assumptions used in developing this model include: (1) the track does not slip on the wheels (i.e., on sprocket, idler, support rollers and road wheels); (2) the track possesses uniform weight/length (ρg) and longitudinal stiffness (EA); (3) the vibration of the lower track spans in contact with the terrain is heavily suppressed.

The boundary and patching conditions required to complete the track circuit model are as follows. Displacement continuity at the wheels (idler wheel, support rollers and sprocket) requires

$$U_i(L_i, T) = U_{i+1}(0, T), \quad i = 1, 2, 3, 4. \tag{13}$$

The moment equations describing the rotation of the discrete elements provide

$$I_i\ddot{\theta}_i = r_i EA[\varepsilon_{d_{i+1}} - \varepsilon_{d_i}], \quad i = 1, 2, 3, 4, \tag{14}$$

where

$$\varepsilon_{d_i} = U_{i,S_i} - \frac{k_i}{L_i} V_i, \tag{15}$$

represents the dynamic strain of the ith track span. By virtue of the quasi-static stretching assumption, the dynamic strains remain uniform within each span, however, they differ in *adjacent* spans contributing to the rotational motion of the attached discrete elements. Through this mechanism, tension fluctuations propagate throughout the circuit. The rotations of the wheels are related to longitudinal span displacements through

$$\theta_i = \frac{U_{i+1}(0, T)}{r_i}, \quad i = 1, 2, 3, 4. \tag{16}$$

The remaining sets of boundary conditions are inhomogeneous and capture excitation sources. Two such sources, roadarm motion and polygonal action, are considered next.

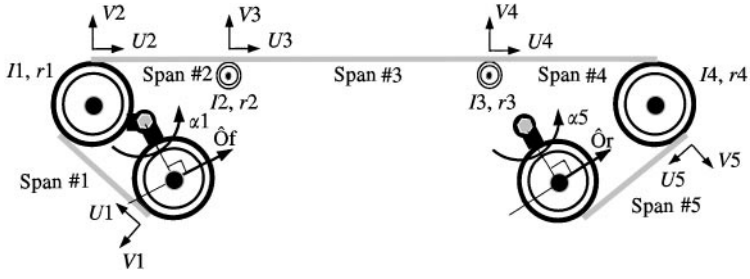

Figure 6. Schematic of upper spans for example vehicle.

TABLE 2

Nomenclature

Variable	Description
U_i, $i = 1, 2, \ldots, 5$	Longitudinal displacement in ith span
V_i, $i = 1, 2, \ldots, 5$	Transverse displacement in ith span
θ_i, $i = 1, 2, \ldots, 4$	Clockwise rotation of ith wheel
L_i, $i = 1, 2, \ldots, 5$	Length of ith span
I_i, $i = 1, 2, \ldots, 4$	Moment of inertia of ith wheel
r_i, $i = 1, 2, \ldots, 4$	Radius of ith wheel

4.1.1. *Roadarm motion*

Prescribed rotations of the front and read road arms, $\alpha_1(T)$ and $\alpha_5(T)$, respectively, generate both transverse and longitudinal motion at the track circuit boundary. The inhomogeneous boundary conditions describing this track excitation are

$$U_1(0, T) = k_{u1}\alpha_1(T), \qquad V_1(0, T) = k_{v1}\alpha_1(T), \tag{17}$$

$$U_5(L_5, T) = k_{u5}\alpha_5(T), \qquad V_5(L_5, T) = k_{v5}\alpha_5(T). \tag{18}$$

With reference to Figure 6, k_{u1} and k_{v1} are determined by the length of the front roadarm and the projection of the unit vector $\hat{o}_f$ onto the directions of U_1 and V_1 respectively. Similarly, the length of the rear roadarm and the projection of the unit vector $\hat{o}_r$ onto the directions of U_5 and V_5 determine the constants k_{u5} and k_{v5} respectively.

4.1.2. *Polygonal action*

As the track engages the sprocket or any circuit wheel, the pitches conform to a polygon rather than a true circle. The instantaneous pitch diameter alternates between that of the inscribed and circumscribed circles of the pitch polygon. This mechanism of "polygonal action" has been well discussed in the literature on chain drives [13–15]. It can lead to chain vibration and to speed fluctuations even with constant speed of the drive sprocket. Using an equivalent four-bar linkage, Lee [15]

models the kinematic effects of polygonal action in a standard chain drive. This concept is extended herein in the context of the track circuit. In this model, the time-harmonic effect of polygonal action is modelled as a prescribed displacement in the transverse direction at the points where the track engages and disengages with the sprocket, idler, and front and rear roadwheels. The inhomogeneous transverse boundary conditions become

$$V_1(0, T) = k_{pfr}\cos(\Omega T + \phi_{fr}), \qquad V_1(L_1, T) = k_{pi}\cos(\Omega T + \phi_i), \tag{19}$$

$$V_2(0, T) = k_{pi}\cos(\Omega T + \phi_i), \qquad V_4(L_4, T) = k_{ps}\cos(\Omega T + \phi_s), \tag{20, 21}$$

$$V_5(0, T) = k_{ps}\cos(\Omega T + \phi_s), \qquad V_5(L_5, T) = k_{prr}\cos(\Omega T + \phi_{rr}). \tag{22}$$

Here, the constants k_{pfr}, k_{pi}, k_{ps}, and k_{prr} are the amplitudes of the polygonal action as defined in Appendix A. Likewise, the quantities ϕ_{fr}, ϕ_i, ϕ_s, and ϕ_{rr} represent the relative phase of the polygonal action; again see Appendix A. Finally, Ω is the frequency of polygonal action given by

$$\Omega = \frac{2\pi V_{tank}}{L_{pitch}}, \tag{23}$$

where V_{tank} is the vehicle speed and L_{pitch} is the track pitch length.

The time dependency of polygonal action above is approximated using the fundamental frequency (pitch passage frequency) and ignoring the higher harmonics that also exist. While one could incorporate these higher harmonics in the very same manner as the fundamental frequency here, one must also recognize the limitations of modelling pitch/sprocket interaction based on *kinematics* alone. Higher fidelity models of this interaction would follow from including the *kinetic* effects associated with the impact of the pitch on the sprocket while seating. Refer, for instance, to impact models used for chain drives [16].

4.2. NATURAL FREQUENCIES AND MODE SHAPES

Consider first the eigenvalue problem governing the natural frequencies and mode shapes of the track circuit. To this end, set the right-hand sides of equations (17)–(22) to zero to define free response.

These boundary conditions are evaluated using the general solutions for the longitudinal and transverse span displacements, equations (9) and (11). Collection of the resulting 20 algebraic equations yields an eigenvalue problem of the form

$$\mathbf{R}(\omega)\cdot\mathbf{a} = \mathbf{0}, \tag{24}$$

where $\mathbf{R}$ is a (20×20) matrix whose elements are functions of ω, and $\mathbf{a}$ is an eigenvector containing the constants A_i, B_i, $\bar{F}_i$, and $\bar{G}_i$, $i = 1, 2, \ldots, 5$. The eigenvalues are determined as the roots of the determinant of $\mathbf{R}$ and are computed using standard Newton–Raphson iteration. The eigenvectors (hence the eigenfunctions) are determined by back substitution of ω into equation (24).

Table 3 summarizes the numerical data that defines the example application discussed in this paper.

Figure 7 illustrates the first four track circuit modes. Each low-order mode shape involves transverse motion largely contained within one span of the circuit with small components in all other spans due to weak coupling across the discrete elements. Accordingly, the fundamental natural frequency of 3·7 Hz can also be closely approximated by the single element method of section 2 applied to a fixed–fixed span with length L_3.

Likewise, the remaining low order modes shown exhibit a response localized to the longer spans. The character of higher order modes follows largely the same pattern of the four shown in Figure 7. However, as the mode number increases, the coupling increases and multiple spans may contribute more significantly to each mode.

It should be recognized that the presence of such low-frequency vibration modes severely limits the range of fidelity of any models employing a massless track (spring) representation. In other words, the bandwidth of any massless track model may be less than 3 Hz for the (typical) application considered here.

TABLE 3

Example

Variable	Description	Value (U.S.)	Value (SI)
EA	Elastic modulus	$2{\cdot}50 \times 10^6$ lb	$11{\cdot}1 \times 10^6$ N
ρ	Track linear density	90·0 lb ft	133·0 kg/m
P_o	Static track tension	14 000 lb	62 364 N
$L_1, \ldots, L_5$	Span lengths	3·39/4·69/9·67/6·48/3·20 ft	1·03/1·43/2·95/1·98/0·98 m
I_1	Idler inertia	9·02 lb–ft–ft	0·38 kg–m–m
$I_{2,3}$	Support roller inertia	2·67 lb–ft–ft	0·11 kg–m–m
I_4	Sprocket inertia	9·66 lb–ft–ft	0·41 kg–m–m
r_1	Idler radius	1·04 ft	0·32 m
$r_{2,3}$	Support roller radius	0·42 ft	0·13 m
r_4	Sprocket radius	1·12 ft	0·34 m

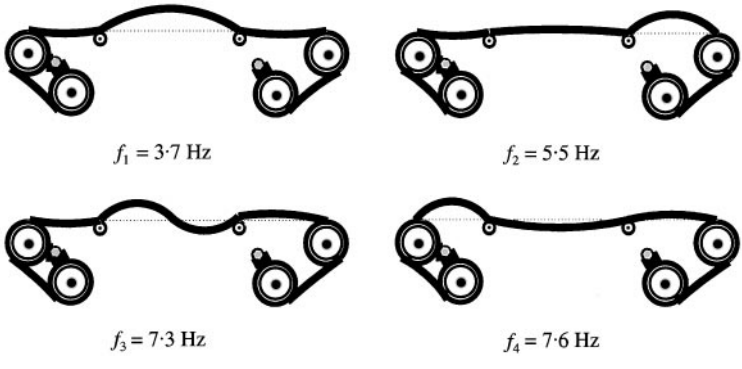

Figure 7. Vibration mode shapes.

4.3. FORCED RESPONSE

The system modes of section 4.2 can be used to calculate the forced response using classical modal analysis. The excitation sources considered are modelled by the inhomogeneous boundary conditions (17)–(22). Incorporation of these boundary conditions involves a variable transformation which employs simple interpolation functions that satisfy the inhomogeneous boundary conditions. Following this transformation, the forced response problem can be formulated as

$$\mathbf{L}[\mathbf{v}^*] + \mathbf{M}[\mathbf{v}^*_{,TT}] = \mathbf{f}, \qquad \mathbf{v}^* = \begin{bmatrix} V_1^*(S_1, T) \\ V_2^*(S_2, T) \\ V_3^*(S_3, T) \\ V_4^*(S_4, T) \\ V_5^*(S_5, T) \\ U_1^*(S_1, T) \\ U_2^*(S_2, T) \\ U_3^*(S_3, T) \\ U_4^*(S_4, T) \\ U_5^*(S_5, T) \end{bmatrix}. \tag{25}$$

Here, $\mathbf{L}$ is a matrix of linear differential operators and $\mathbf{M}$ is a matrix of scalars. The vector $\mathbf{v}^*$ contains five functions representing the transverse span displacements, and five functions representing the rotation of each wheel. The elements within $\mathbf{v}^*$ are transformations of the span displacement functions and satisfy homogeneous boundary conditions. The vector $\mathbf{f}$ contains the by-products of this transformation, the details of which are included in Appendix A. The response vector $\mathbf{v}^*$ can be expanded using an infinite number of modes as follows:

$$\mathbf{v}^* = \sum_{j=1}^{\infty} \beta_j(T)\bar{\mathbf{v}}_j, \qquad \bar{\mathbf{v}}_j = \begin{bmatrix} \bar{V}_1(S_1) \\ \bar{V}_2(S_2) \\ \bar{V}_3(S_3) \\ \bar{V}_4(S_4) \\ \bar{V}_5(S_5) \\ \bar{G}_1 \\ \bar{G}_2 \\ \bar{G}_3 \\ \bar{G}_4 \\ \bar{G}_5 \end{bmatrix}_j, \tag{26}$$

where β_j is the jth modal co-ordinate. The (decoupled) equations governing the modal co-ordinates are found through substitution of equation (26) into equation (25) and forming an inner-product with the mode $\bar{\mathbf{v}}_k$,

$$\sum_{j=1}^{\infty} [\beta_j \langle \mathbf{L}[\bar{\mathbf{v}}_j], \bar{\mathbf{v}}_k \rangle + \ddot{\beta}_j \langle \mathbf{M}[\bar{\mathbf{v}}_j], \bar{\mathbf{v}}_k \rangle = \langle \mathbf{f}, \bar{\mathbf{v}}_k \rangle]. \tag{27}$$

The inner product of two eigenvectors $\bar{\mathbf{v}}_j$ and $\bar{\mathbf{v}}_k$ is defined as

$$\langle \bar{\mathbf{v}}_j, \bar{\mathbf{v}}_k \rangle = \sum_{i=1}^{5} \int_0^{L_i} \bar{V}_{i_j}(S_i) \bar{V}_{i_k}(S_i) \, \mathrm{d}S_i + \bar{G}_{i_j} \bar{G}_{i_k}]. \tag{28}$$

The modes are orthogonal with respect to the operators **L** and **M** and equation (27) reduces to the decoupled modal equations

$$\ddot{\beta}_j + \omega_j^2 \beta_j = Q_j(T), \quad j = 1, 2, \ldots, \tag{29}$$

$$Q_j(T) = \frac{\langle \mathbf{f}, \bar{\mathbf{v}}_j \rangle}{\langle \mathbf{M}[\bar{\mathbf{v}}_j], \bar{\mathbf{v}}_j \rangle}, \tag{30}$$

where ω_j is the jth *system* natural frequency and $Q_j(T)$ is the contribution of the forcing to the jth mode. At this stage, it is possible to add appropriate levels of damping to each mode through obvious modification of equation (29). The decoupled set of equations (29) are readily integrated in time for each selected mode and the response vector $\mathbf{v}^*$ can then be reconstructed using equation (26). The track responses presented here will be expanded using the first 8 system modes, the eighth of which has a frequency of approximately 12 Hz, and are also based on using a modal damping factor of 5% of critical damping.

4.4. EXAMPLE RESULTS

Three example excitation mechanisms will be used to illustrate characteristics of track vibration. First, a pure harmonic excitation is used to determine the track circuit frequency response. Second, the effects of polygonal action will be investigated in the context of a vehicle traversing flat terrain. Lastly, the track response to the excitation encountered as a tank travels over an example bump course will be shown.

4.4.1. *Excitation* 1: *frequency response*

Consider the input to the track circuit to be a prescribed harmonic longitudinal displacement at the front roadwheel. The frequency of the harmonic displacement may vary from 0 to 14 Hz for the purpose of exciting low order track modes while the amplitudes of the displacement is held constant at 0·1 ft (3·05 cm). Figure 8 illustrates the track frequency response using the mid-span transverse response amplitude of the five spans as one measure of the output.

The clear resonances in Figure 8 coincide with the circuit natural frequencies reported in Figure 7 as required. The longest track span, span 3, dominates the response in the first resonance and, in order of decreasing length, the other spans dominate the subsequent resonances. The longest span remains the *softest* span of the circuit and therefore the response magnitude will increase with any increase in span length. Note that the coupling between longitudinal and transverse motions captured by the element model allows transverse response to be excited with pure longitudinal input.

4.4.2. *Excitation* 2: *polygonal action*

Transverse input of course directly excites transverse track response. One mechanism that generates transverse input is polygonal action. To illustrate this, consider a vehicle traversing nominally flat terrain at various speeds ranging up to 7 mph (11·3 kph). The results in Figure 9 illustrate the track frequency response; refer to equation (23) and note that the excitation frequency Ω is directly proportional to the track speed. As before, the (steady state) mid-span transverse response amplitude of the five circuit spans is used as the output. In Figure 9, the span resonances occur at track speeds that directly correlate to the resonance frequencies of Figure 8. The response magnitude is greatest for span 5 due to its location between the sprocket and rear roadwheel, two major sites of excitation from polygonal action. By contrast, span 3 exhibits very little response as it remains well isolated from the sites

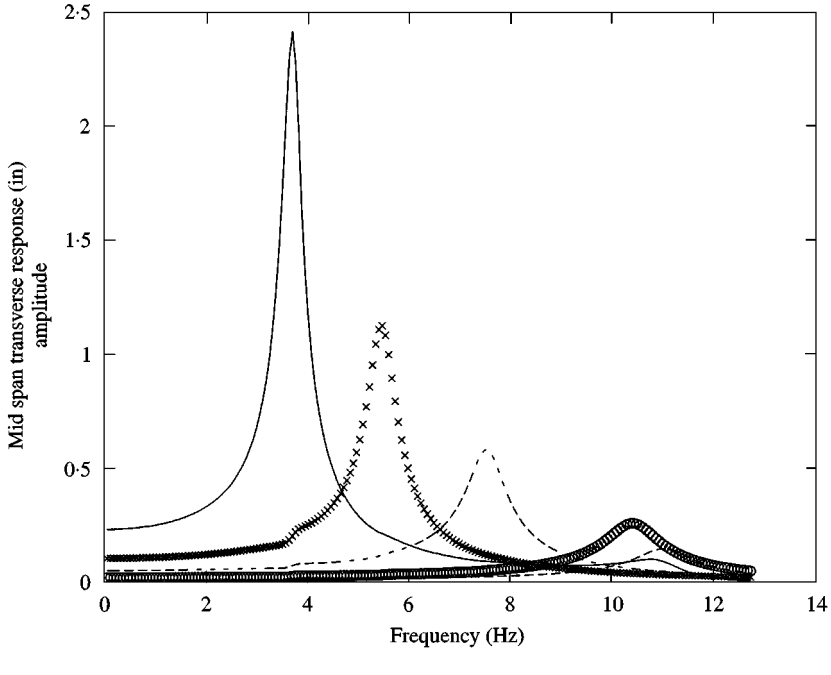

Figure 8. Track frequency response to harmonic longitudinal excitation at front road wheel: ○○○○, span 1; — - — - —, span 2; ——, span 3; × × × ×, span 4; – – – –, span 5.

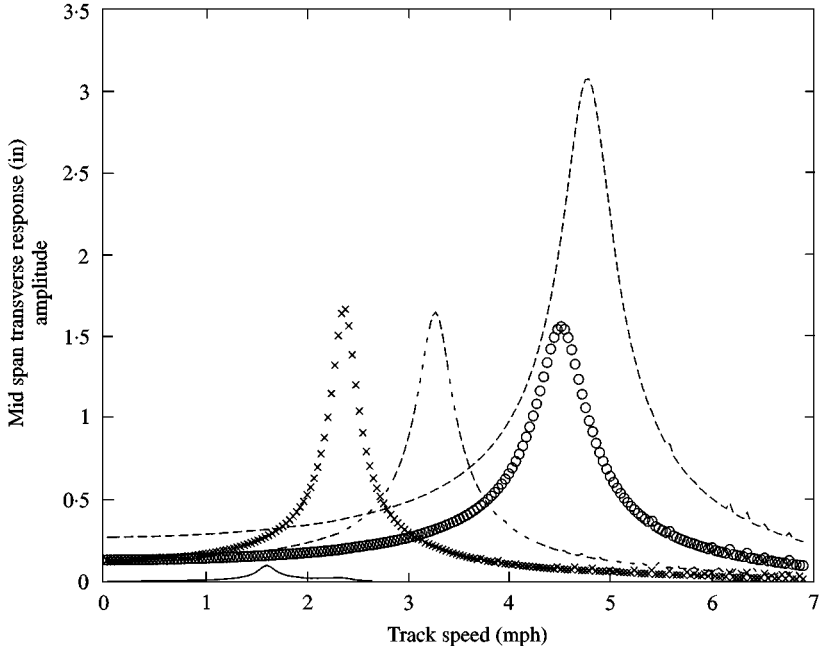

Figure 9. Track frequency response to polygonal action: ○○○○, span 1; — - — - —, span 2; ——, span 3; × × × ×, span 4; – – – –, span 5.

where polygonal action exists. The overall vibration amplitudes at resonance, ranging from 1·5 to 3·0 in (3·8–7·6 cm), are on the order of the static sag for a given span sagging under its own weight. Thus, even in the seemingly benign case of traversing flat terrain at low speeds, significant track vibration exists.

4.4.3. *Excitation* 3: *bump course*

Clearly, a major source of track vibration is the response of the vehicle to uneven terrain. One mechanism for producing this vibration is the response of the track to the rotations of the front and rear roadwheels/roadarms. This example illustrates this mechanism by employing example front and rear roadarm motions first computed using an established tracked vehicle code.† The computed roadarm motions are then used to drive the upper-span track vibration model developed herein through boundary conditions (17)–(18). The roadarm motions are those developed for the example tracked vehicle traversing an uneven paved road course at a constant speed of 11 mph (17·7 kph). The course contains a series of 4·5 in (11·4 cm) and 6 in (15·2 cm) high trapezoidal obstacles spaced approximately 35 ft apart.

Figure 10(a) illustrates the front roadarm angle time history, the spectral content of which appears in Figure 10(b). Figure 11(a) illustrates the mid-span transverse

† Tracked vehicle code is based on the track super-element [4] with results provided by J. Weller from U.S. Army TACOM.

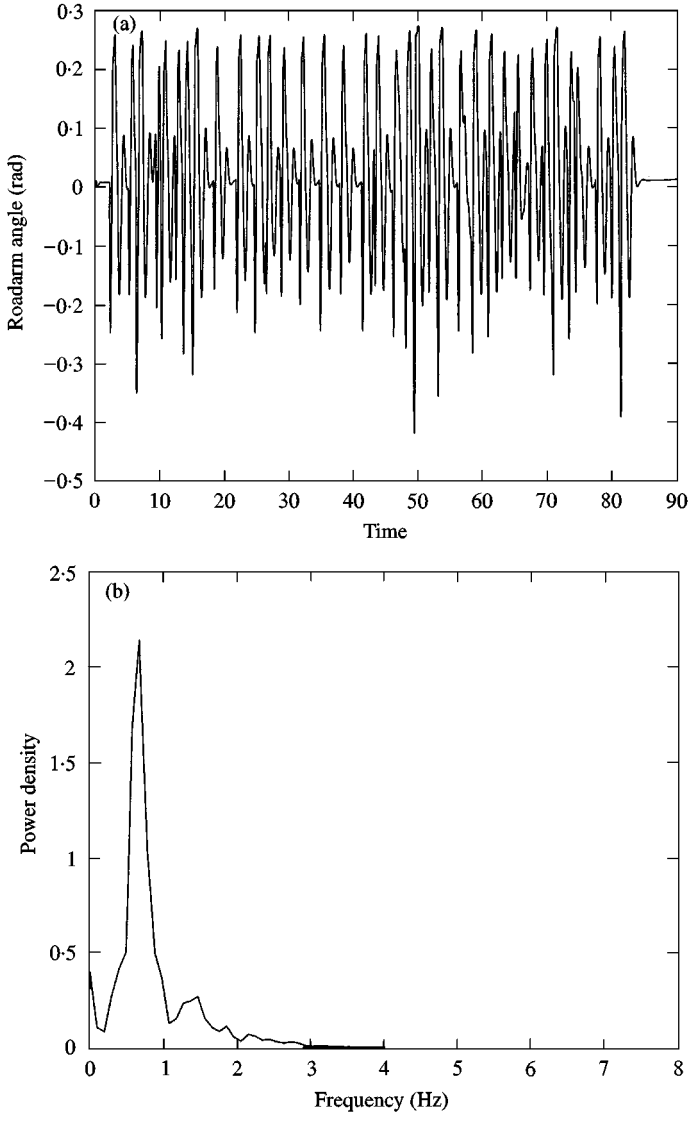

Figure 10. Bump course input: (a) front roadarm input; (b) input power spectral density.

response of span 3 over the 90 s simulation. The maximum transverse displacement of this span, approximately 5 in, is sufficiently large to create impact of the track with the underside of the hull (sponson). Furthermore, the pitch and bounce motions of the vehicle as it crosses such a course, though not presently represented here as an excitation source, would likely contribute substantial additional energy to the low order circuit modes.

The zoom view of the time response, Figure 11(b), illustrates two distinct vibration frequencies. One occurs at approximately 3·7 Hz, the frequency of the fundamental circuit mode, and superimposed upon it is the pitch passing

frequency of approximately 25 Hz. The pitch passing frequency correlates directly with the effect of polygonal action at a track speed of 11 mph (17·7 kph). The spectral content of the response is illustrated in Figure 11(c). Much of the response energy remains below 5 Hz and this suggests that a two-mode model of the track would successfully capture the essential features of track vibration in this case. Such a low order model of the track would clearly benefit any effort to compute real-time track response over a bandwidth including track vibration.

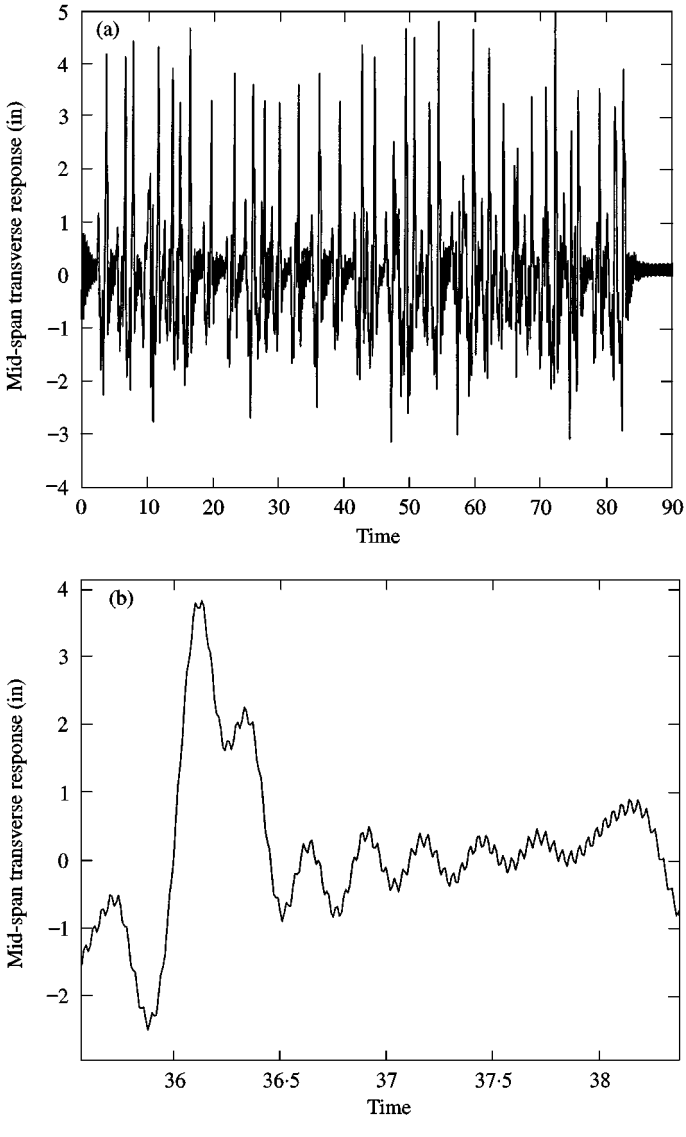

Figure 11. Bump course responses: (a) mid-span response of span 3; (b) zoom view; (c) response power spectral density.

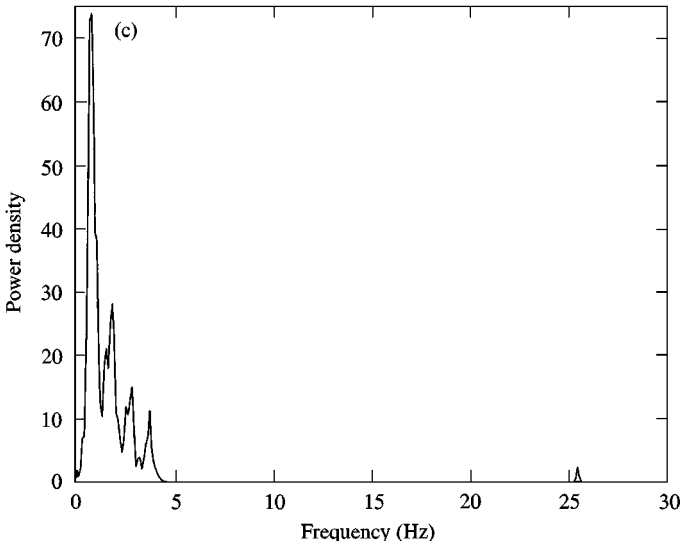

Figure 11. Continued

5. SUMMARY AND CONCLUSIONS

There is a need for low order tracked vehicle models that capture the essential features of track vibration. Existing multi-body dynamic track models capture track vibration, however, they do so at the expense of model size; i.e., large d.o.f. This paper offers an alternative modelling strategy, based on a continuum model for the track, that leads to low-order track models.

In contrast to a multi-body approach, the track spans are modelled herein as continuum elements that describe both longitudinal (quasi-static) and transverse modes of vibration. Experiments on a representative track span support the use of the continuum element model for low order track vibration modes. A track circuit model, composed of multiple spans coupled to the remaining rigid-body elements of the track circuit, is developed by repeated use of the element model. An eigenanalysis of the circuit model leads to the track system modes that are subsequently employed in computing forced response. The natural frequency of the fundamental system mode (calculated to be approximately 3 Hz in the example) places severe restriction on the range of fidelity of models employing a massless track representation.

Principal characteristics of track vibration are evaluated by considering excitation from (1) roadarm motion and (2) polygonal action. Results for a vehicle traversing level terrain indicate that notable track vibration levels exist from polygonal action alone. Both excitation sources are active as the vehicle traverses uneven terrain. Results from an example bump course reveal that track response decomposes into vibration due to polygonal action (relatively high frequency) and vibration due to terrain-induced roadarm motion (relatively low frequency). The associated power spectrum suggests that track vibration response is well described using just two system modes for the example herein.

Employing low order system modes to describe track vibration is an efficient alternative to conventional multi-body modelling methods. To this end, the authors' research group has implemented this track model within a full tracked vehicle model, the results of which will be the subject of a forthcoming article. The resulting full vehicle model could provide rapid estimates of track vibration response and prove useful for evaluating tracked vehicle designs and for supporting real-time vehicle simulation.

ACKNOWLEDGMENTS

The authors acknowledge support provided by the U.S. Army Tank-Automotive Command (TACOM) through the University of Michigan Automotive Research Center, a U.S. Army Center of Excellence for Automotive Research, under contract number DAAE07-94-C-R094. The authors gratefully acknowledge Mr Mike Saxon (formerly of U.S. Army TACOM) for providing the experimental results in support of section 3 and Mr John Weller (U.S. Army TACOM) for providing the example roadarm inputs used in section 4.4.

REFERENCES

1. P. Wheeler 1977 *SAE Paper No.* 770048. Tracked vehicle ride dynamics computer program.
2. M. R. Garnich and T. R. Grimm 1984 *ASME Proceedings of the International Computers in Engineering Conference and Exhibit on Advanced Automation* **2**, 591–600. Modeling and simulation of a tracked vehicle.
3. M. D. Bennett and P. H. G. Penny 1985 *IMech Conference Publications 1985-5* C112/85, 103–117. The assessment of tracked vehicle suspensions using computer simulation techniques.
4. E. J. Haug and M. K. McCullough 1985 *Transactions of the American Society of Mehanical Engineers, Journal of Mechanisms, Transmissions, and Automation in Design* **85-DET-95**, 1–8. Dynamics of high mobility track vehicles.
5. A. Dhir and S. Sankar 1994 *Vehicle System Dynamics* **23**, 379–409. Ride dynamics of high-speed tracked vehicles: simulation with field validation.
6. J. H. Choi 1996 *Ph.D. Thesis, University of Illinois at Chicago*. Use of recursive and approximation methods in the dynamic analysis of spatial tracked vehicles.
7. J. P. Wilcox 1989 *U.S. Army Engineer Waterways Experiment Station Report*. Documentation for the Trackdyne II Program.
8. J. P. Wilcox 1994 *U.S. Army Engineer Waterways Experiment Station Report*. Documentation for the Trackdrive Program.
9. A. G. Galaitsis 1984 *Transactions of the American Society of Mechanical Engineers, Journal of Vibration, Acoustics, Stress, and Reliability in Design* **106**, 286–291. TRAXION: a model for predicting dynamics track loads in military vehicles.
10. H. M. Irvine and T. K. Caughey 1974 *Proceedings of the Royal Society, London* **A-341**, 299–315. The linear theory of free vibrations of a suspended cable.
11. N. C. Perkins 1992 *International Journal of Non-linear Mechanics* **27**, 233–250. Modal interactions in the nonlinear response of elastic cables under parametric/external excitation.
12. C. Scholar and N. C. Perkins 1997 *SAE Paper No.* 971090. Longitudinal vibration of elastic vehicle track systems.
13. S. Mahalingham 1958 *Journal of Franklin Institute* **265**, 23–28. Polygonal action in chain drives.

14. C. K. Chen and F. Freudenstein 1988 *Journal of Mechanisms, Transmissions, and Automation in Design* **110**, 269–275. Toward a more exact kinematics of roller chain drives.
15. T. H. Lee 1983 *Journal of Mechanisms, Transmissions, and Automation in Design* **105**, 362–370. Automated dynamic analysis of chain-driven mechanical systems.
16. K. W. Wang, S. P. Liu, S. I. Hayek and F. H. K. Chen 1992 *Transactions of the American Society of Mechanical Engineers, Journal of Vibration and Acoustics* **114**, 397–403. On the impact intensity of vibrating axially moving roller chains.

APPENDIX A: MATRIX EXPRESSIONS

The inhomogeneous boundary conditions due to roadarm motions and polygonal action are satisfied through the following variable transformation:

$$V_1(S_1, T) = V_1^*(S_1, T) + [k_{v1}\alpha_1(T) + k_{pfr}\cos(\Omega T + \phi_{fr})]\left[1 - \frac{S_1}{L_1}\right] + k_{pi}\cos(\Omega T + \phi_i)\left[\frac{S_1}{L_1}\right], \tag{A1}$$

$$V_2(S_2, T) = V_2^*(S_2, T) + k_{pi}\cos(\Omega T + \phi_i)\left[1 - \frac{S_2}{L_2}\right], \tag{A2}$$

$$V_3(S_3, T) = V_3^*(S_3, T), \tag{A3}$$

$$V_4(S_4, T) = V_4^*(S_4, T) + k_{ps}\cos(\Omega T + \phi_s)\left[\frac{S_4}{L_4}\right], \tag{A4}$$

$$V_5(S_5, T) = V_5^*(S_5, T) + [k_{v5}\alpha_5(T) + k_{prr}\cos(\Omega T + \phi_{rr})]\left[\frac{S_5}{L_5}\right] + k_{ps}\cos(\Omega T + \phi_s)\left[1 - \frac{S_5}{L_5}\right], \tag{A5}$$

$$U_1(S_1, T) = U_1^*(S_1, T) + k_{u1}\alpha_1(T)\left[1 - \frac{S_1}{L_1}\right], \tag{A6}$$

$$U_2(S_2, T) = U_2^*(S_2, T), \qquad U_3(S_3, T) = U_3^*(S_3, T), \qquad U_4(S_4, T) = U_4^*(S_4, T). \tag{A7–A9}$$

$$U_5(S_5, T) = U_5^*(S_5, T) + k_{u5}\alpha_5(T)\left[\frac{S_5}{L_5}\right]. \tag{A10}$$

The constants k_{pfr}, k_{pf}, k_{ps}, and k_{prr} are the amplitudes of the polygonal action at the front roadwheel, idler, drive sprocket and rear roadwheel respectively. These

amplitudes are determined by

$$k_p = \frac{R[1 - \cos(\sin^{-1}[L_{pitch}/2R])]}{2}, \tag{A11}$$

where L_{pitch} is the track pitch length and R is the wheel radius at the site of polygonal action. The quantities ϕ_{fr}, ϕ_i, ϕ_s, and ϕ_{rr} are the relative phases of the polygonal action at the front roadwheel, idler, drive sprocket and rear roadwheel respectively. Time phasing between the action at different sites within the circuit is accounted for by calculation of the fractional number of pitches which lie in adjacent track spans. An integral number of pitches yields exactly in-phase excitation while an odd number of half-pitches yields a phase angle of π.

The linear interpolation functions appearing above satisfy the non-homogeneous boundary conditions (17)–(22) and the remaining variables, V_i^*, U_i^*, $i = 1, 2, \ldots, 5$ satisfy *homogeneous* boundary conditions. These variables are then expanded in an eigenfunction expansion as per section 4.3.

When these solution forms are substituted into equations of motion (2) and (14), the resulting set of equations are given by equation (25) with the operators **L** and **M** defined as

$$\mathbf{L} = \begin{bmatrix} a_1 & 0 & 0 & 0 & 0 & b_1 & 0 & 0 & 0 & 0 \\ a_2 & 0 & 0 & 0 & 0 & b_2 & 0 & 0 & 0 & 0 \\ a_3 & 0 & 0 & 0 & 0 & b_3 & 0 & 0 & 0 & 0 \\ a_4 & 0 & 0 & 0 & 0 & b_4 & 0 & 0 & 0 & 0 \\ a_5 & 0 & 0 & 0 & 0 & b_5 & 0 & 0 & 0 & 0 \\ 0 & 0 & 0 & 0 & 0 & 0 & 0 & 0 & 0 & 0 \\ -a_1' & a_2' & 0 & 0 & 0 & b_1' & -b_2' & 0 & 0 & 0 \\ 0 & -a_2' & a_3' & 0 & 0 & 0 & b_2' & -b_3' & 0 & 0 \\ 0 & 0 & -a_3' & a_4' & 0 & 0 & 0 & b_4' & -b_4' & 0 \\ 0 & 0 & 0 & -a_4' & a_5' & 0 & 0 & 0 & b_4' & -b_5' \end{bmatrix}, \quad \mathbf{M} = \begin{bmatrix} \mathbf{C} & \mathbf{0} \\ \mathbf{0} & \mathbf{D} \end{bmatrix}, \tag{A12, A13}$$

where

$$\mathbf{C} = \begin{bmatrix} \frac{1}{g} & 0 & 0 & 0 & 0 \\ 0 & \frac{1}{g} & 0 & 0 & 0 \\ 0 & 0 & \frac{1}{g} & 0 & 0 \\ 0 & 0 & 0 & \frac{1}{g} & 0 \\ 0 & 0 & 0 & 0 & \frac{1}{g} \end{bmatrix}, \qquad \mathbf{D} = \begin{bmatrix} d_1 & 0 & 0 & 0 & 0 \\ 0 & \dfrac{I_1}{r_1^2} d_2 & 0 & 0 & 0 \\ 0 & 0 & \dfrac{I_2}{r_2^2} d_3 & 0 & 0 \\ 0 & 0 & 0 & \dfrac{I_3}{r_3^2} d_4 & 0 \\ 0 & 0 & 0 & 0 & \dfrac{I_4}{r_4^2} d_5 \end{bmatrix}, \tag{A14, A15}$$

$$a_i = \left[\frac{k_i^2 v_{li}^2}{L_i} \square - v_{ti}^2 L_i \square_{,S_i,S_i} \right], \qquad b_i = [-k_i v_{li}^2 \square_{,S_i}], \tag{A16, A17}$$

$$a_i' = \frac{k_i}{L_i} \square, \qquad b_i' = \square_{,S_i}, \qquad d_i = \square|_{S_i = 0}. \tag{A18–A20}$$